UWL REPOSITORY

repository.uwl.ac.uk

Ultrafine platinum nanoparticles supported on covalent organic frameworks as stable and reusable oxidase-like catalysts for cellular glutathione detection

Jin, Peng, Niu, Xiaoying, Gao, Zixi, Xue, Xuqi, Zhang, Fang, Cheng, Wei, Ren, Cuiling, Du, Hongying, Manyande, Anne ORCID logoORCID: https://orcid.org/0000-0002-8257-0722 and Chen, Hongli (2021) Ultrafine platinum nanoparticles supported on covalent organic frameworks as stable and reusable oxidase-like catalysts for cellular glutathione detection. ACS Applied Nano Materials, 4 (6). pp. 5834-5841.

This is the Accepted Version of the final output.

Ultrafine Platinum Nanoparticles Supported on Covalent Organic Frameworks as Stable and Reusable Oxidase-Like Catalysts for Cellular Glutathione Detection

Peng Jin[†,∥], Xiaoying Niu[§,∥], Zixi Gao[†], Xuqi Xue[†], Fang Zhang[†], Wei Cheng[†],

Cuiling Ren[†], Hongying Du[‡], Anne Manyande[⊥], and Hongli Chen[†,*]

[†] State Key Laboratory of Applied Organic Chemistry, College of Chemistry and Chemical Engineering, Lanzhou University, Lanzhou 730000, China

[‡] Key Laboratory of Environment Correlative Dietology, Ministry of Education, College of Food Science and Technology, Huazhong Agricultural University, Wuhan, Hubei, China

[§] College of Chemistry and Environmental Science, Key Laboratory of Analytical Science and Technology of Hebei Province, and MOE Key Laboratory of Medicinal Chemistry and Molecular Diagnostics, Hebei University, Baoding, Hebei, China

[⊥] School of Human and Social Sciences, University of West London, London, UK

✉ Hongli Chen

   hlchen@lzu.edu.cn

✉ Hongying Du

   hydu@mail.hzau.edu.cn

[∥] Theri contributions to this article are equal.

1

ABSTRACT

Nanozymes have been widely developed as supplements of natural enzymes owing to the relatively low cost, high mass production, easy storage, good stability and reusability. By controlling the particle size, nanozymes' catalytic activities can distinctly be improved. The porous materials such as covalent organic framework (COF) are definitely considered as promising supports for in-situ preparing high dispersity and small size of nanozymes. Herein, we designed and synthesized COF-supported ultrafine platinum nanoparticles (PtNPs/COF-300-AR) by controlling the growth of Pt NPs in virtue of uniformly distributed nitrogen atoms of well-organized framework structures of 3D COF. PtNPs/COF-300-AR nanohybrids catalyzed the colorless 3,3',5,5'-tetramethylbenzydine (TMB) solution to turn blue, displaying excellent oxidase-like activity, good stability and high reusability, which should be owed to the uniform size and high dispersity of ultrafine Pt NPs. By virtue of those advantages, the TMB-PtNPs/COF-300-AR colorimetric platform was successfully applied to cellular glutathione detection. Similarly, other COFs with good acid resistance and abundant functional groups can also be used as the supports of nanozyme, which will greatly expand the members of the nanoenzyme family.

KEYWORDS: *oxidase mimic*, *in-situ preparation*, *ultrafine Pt nanoparticles*, *COF support*, *glutathione, nanohybrids, colorimetry, cell lysate*

2

1. INTRODUCTION

Since it was first reported that Fe_3O_4 nanoparticles have the intrinsic peroxidase-like catalytic capacity in 2007 by Gao et al.,[1] extensive research about nanozymes (i.e. nanomaterial-based enzyme mimics) has been carried out. Compared to natural enzymes, nanozymes own outstanding strengths including low cost, high mass production, convenient storage, good stability and reusability, being recognized by experts from different fields and widely applied to immunoassays, chemical and biomedical sensing, nerve protection, disease diagnostics and other fields.[2,3]

Until now, a variety of nanozymes have been designed and fabricated, for instance, iron-based,[1,4-8] noble metal-based,[9-14] metal oxide-based,[15-18] carbon-based,[19-22] porous materials-based,[23-30] and even some composite nanozymes comprised of several nanomaterials.[31-35] Generally, the nanozymes can mimic one or more of four classes of redox enzymes including oxidase, peroxidase, superoxide dismutase and catalase. Among them, noble metal nanoparticles (NPs) like Pt NPs have superior enzyme-like catalytic performance.[35,36-38] Upon most occasions, the nanozymes with smaller size have higher catalytic activity.[39,40] However, to obtain Pt NPs with small size (< 5 nm) and high dispersibility is a challenging work due to the easy aggregation property.

Covalent organic framework (COF), as a representative class of porous materials, has been developed as excellent support to in-situ synthesis and immobilize noble metal NPs.[41-47] Not surprising, these COF-supported NPs exhibited uniform size and morphology and outstanding catalytic performance. For example, Lu and co-workers designed a thioether-containing COF, and immobilized ultrafine Pd NPs and Pt NPs

3

inside the COF cavity, providing excellent catalytic activities in Suzuki-Miyaura coupling reaction and nitrophenol reduction, respectively.[43] However, it is very difficult to apply these nanohybrids as enzyme-like catalyst due to the poor acid tolerance of COF template. In our previous work, the imine-linkage COF-300 was reduced by $NaBH_4$ to the amine-linkage COF-300-AR, which presented excellent light-responsive oxidase-like activity, high stability and good reusability despite harsh experiment conditions.[30] Since the amine-type ligand is highly effective toward the combination of varied metal ions,[42,48,49] stable COF-300-AR could be an ideal template for immobilizing noble metal NPs with small size and narrow distribution due to the interconnected pores, which can provide superior enzyme-like catalytic performance.

Here, we designed and in-situ synthesized COF-supported ultrafine Pt NPs as oxidase mimic. The ultrafine Pt NPs around 2.2 nm was immobilized on the surface of COF-300-AR template utilizing uniformly distributed nitrogen atoms of the ordered framework structures. The COF-supported Pt NPs (PtNPs/COF-300-AR) showed predominant oxidase-like catalytic activities to the oxidation reaction of 3,3',5,5'-tetramethylbenzydine (TMB), with the advantages including rich catalytic sites, good stability and high reusability. Some reductive substances, such as glutathione (GSH), can suppress TMB oxidation, causing blue color to fade and absorption intensity to reduce. Therefore, PtNPs/COF-300-AR had been developed as a reliable sensor for the detection of cellular GSH level.

4

2. MATERIALS AND METHODS
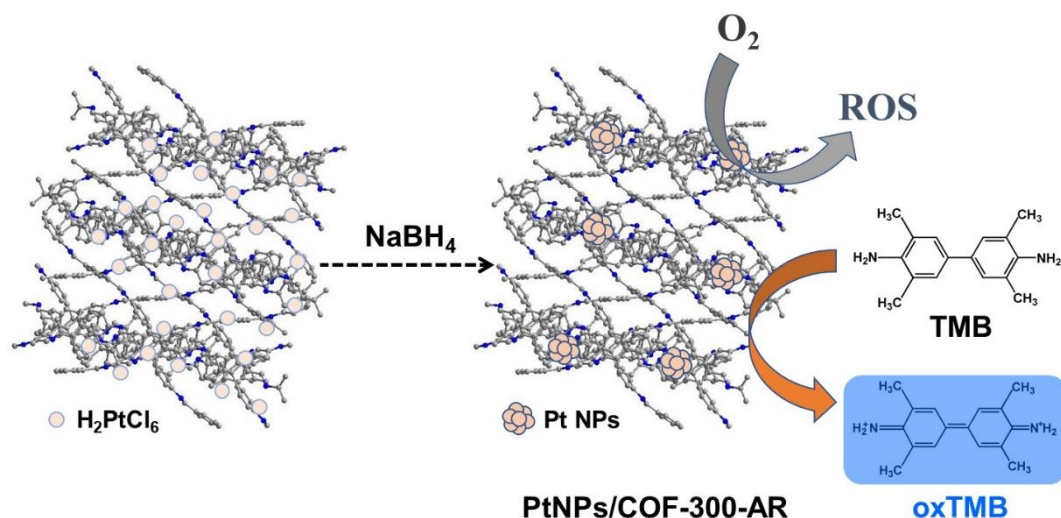
Scheme 1. The preparation process of PtNPs/COF-300-AR and its oxidase-like catalytic application for TMB oxidation.

Scheme 1 presents the synthetic process of PtNPs/COF-300-AR. First, COF-300-AR (75 mg) was dispersed well in distilled water (10 mL), then chloroplatinic acid (10 mg, 19.3 μmol) was added and stirred at room temperature for 3 h. Secondly, solid NaBH$_4$ (0.2 g, 5.29 mmol) was slowly added in small amount within 5 min and stirred for 1 d. Finally, the gray solid (named as PtNPs/COF-300-AR) was collected by centrifugation, washed three times with water and ethanol, and dried in vacuum (60 °C).

The other experimental processes are provided in Supporting information, which is similar to our previous work.[30]

3. RESULTS AND DISCUSSION

3.1. Characterization of PtNPs/COF-300-AR.

To obtain a more stable COF template to in-situ prepare ultrafine Pt NPs, the

5

imine-linkage COF-300 was firstly reduced to amine-linkage COF-300-AR according to previously reported works.[30,50] As shown in FT-IR spectra (Fig. S1), the benzylidene aniline peak of COF-300 at 1620 cm^{-1} disappeared, and the benzyl aniline peaks of COF-300-AR at 1251 and 1608 cm^{-1} appeared, indicating a successful reduction. Although the crystal structure changed from the *dia-c5* topology of COF-300 to the collapsed hydrated form of COF-300-AR after the reduction reaction,[30] amine-linked COF kept structural integrity and showed good compatibility with acidic condition (Fig. 1A, blue line). After in-situ preparation of Pt NPs with NaBH$_4$ reduction, the PXRD pattern of PtNPs/COF-300-AR (Fig. 1A, green line) was consistent with that of COF-300-AR except new peaks appearing at $2\theta = 40°$, $46°$ and $68°$ assigned for (111), (200) and (220) planes of unsupported Pt NPs (Fig. S2), demonstrated the integrity and crystallinity of COF were well retained in the process of successful loading Pt NPs.[43]

TEM image (Fig. 1B) and SEM image (Fig. S3) of PtNPs/COF-300-AR showed that ultrafine Pt NPs evenly spread on the surface of COF template. The medium diameter of Pt NPs was 2.2 nm with a narrow size distribution, which was basically consistent with the average diameter of 2.3 nm calculated from the (111) plane of Pt NPs in PXRD pattern using the Scherrer formula. The few Pt NPs with diameters larger than 2.3 nm may be due to partial aggregation. Compared with unsupported Pt NPs (Fig. S4), it was obvious that COF-300-AR was a beneficial template for forming ultrafine Pt NPs. We found the dosage of Pt source had vital effect on the number, size and dispersity of the in-situ prepared Pt NPs. When H$_2$PtCl$_6$·6H$_2$O dosage was 10 mg, the Pt NPs was small size and high dispersion. However, with the increase in the dosage

6

of Pt source (25 mg or 50 mg), the size of Pt NPs increased and their aggregation become more frequently (Fig. S5). To save Pt source and obtain ultrafine Pt NPs with high enzyme-like catalytic activity, 10 mg $H_2PtCl_6 \cdot 6H_2O$ was selected.

SAED pattern (Fig. 1C) presented the characteristic diffraction ring of COF-supported Pt NPs, and high resolution TEM image (Fig. S6) also confirmed that Pt NPs were highly crystalline, which are coincident with the result from PXRD profile (Fig. 1A, green line). Next, EDS elemental mappings (Fig. 1D and Fig. S7) displayed that the constituent elements including Pt, C, N and O were all uniformly distributed on PtNPs/COF-300-AR, which once more confirms the high dispersity of Pt NPs on template COF-300-AR. The Pt content in PtNPs/COF-300-AR was 2.52% (w/w) by ICP-OES analysis ($n = 3$), which was almost half the added Pt content (4.44%, w/w) during the synthesis. After loading Pt NPs, the measured BET surface area and pore size of the nanohybrids were basically consistent with the COF-300-AR support (Fig. S8), which verified that Pt NPs (~2.2 nm) mainly distributed on the surface of COF-300-AR template.
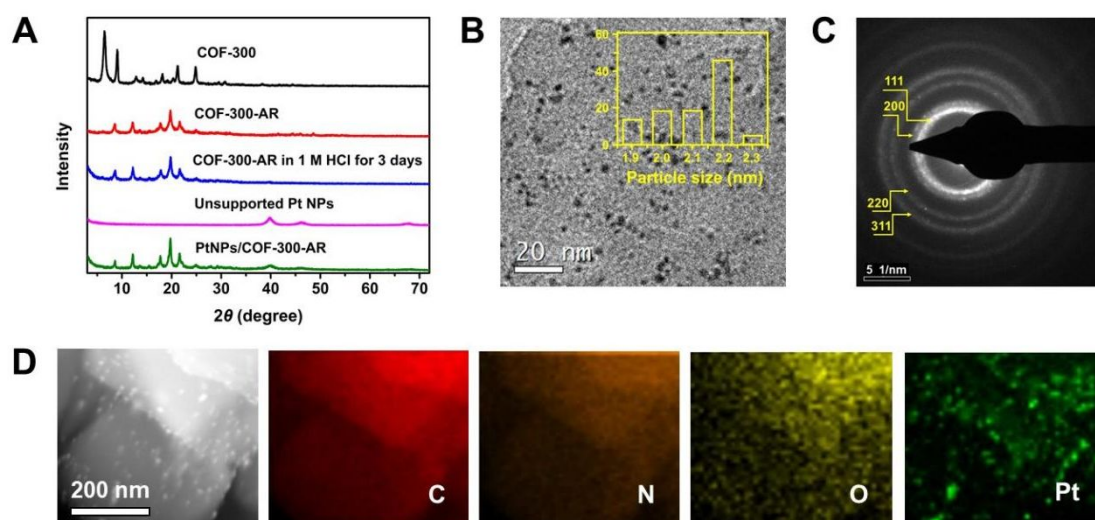

7

Figure 1. Characterizations of PtNPs/COF-300-AR with 10 mg $H_2PtCl_6 \cdot 6H_2O$ as Pt source: (A) PXRD patterns; (B) TEM image, the inset is size distribution histogram of Pt NPs based on about 100 nanoparticles; (C) SAED pattern; (D) EDS mapping.

Furthermore, the element composition (Pt, C, N, O) of PtNPs/COF-300-AR evaluated by XPS spectrum (Fig. 2A) and EDS mapping was in good agreement. The Pt 4f region consisted of a higher energy band (Pt $4f_{5/2}$) and a lower one (Pt $4f_{7/2}$). From Fig. 2B, the doublets can be divided into two pairs (Pt^0 and Pt^{2+} species): (1) Pt^0 species, including Pt $4f_{5/2}$ (74.6 eV) and Pt $4f_{7/2}$ (71.3 eV); (2) Pt^{2+} species, including Pt $4f_{5/2}$ (75.6 eV) and Pt $4f_{7/2}$ (72.1 eV). The ratio of Pt^0/Pt^{2+} is 0.89 based on the peak area. The reoxidation of Pt^0 species should be responsible for the existence of Pt^{2+} species, which has previously been found after exposing nanoparticles to air.[43]
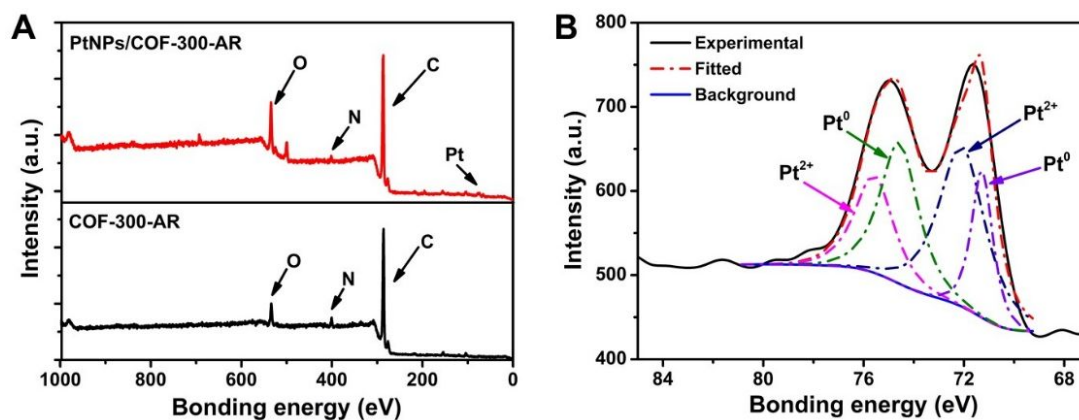

Figure 2. (A) The XPS spectra. (B) Pt$_{4f}$ region in the XPS spectrum of PtNPs/COF-300-AR.

To sum up, Pt NPs with small size (~2.2 nm) and high dispersity had been successfully in-situ prepared on the surface of COF-300-AR support. As known, the ultrafine Pt NPs are superior redox enzyme mimic,[2,3] and COF-300-AR has enough

acid resistance,[30] which guaranteed that our prepared PtNPs/COF-300-AR can be an

excellent oxidase mimic.

3.2. Oxidase-Like Catalytic Activity of PtNPs/COF-300-AR.

In the work, 2,2'-azino-bis(3-ethylbenzothiazoline-6-sulffonicacid) (ABTS) and

3,3',5,5'-tetramethylbenzidine (TMB) were employed as the representative substrates.

As seen from Fig. S9, the characteristic peaks were found at 652 nm and 417 nm,

respectively, indicating that the hybrid materials catalyzed the oxidation of TMB and

ABTS to generate colored products. Moreover, the catalytic activity was also affected

by multi-factors including solution pH, reaction time and temperature, enzyme and

substrate concentrations, which is like a natural oxidase. As shown in Fig. S10, the

optimal conditions were as following: 50 μg/mL PtNPs/COF-300-AR, 133 μM TMB,

reaction time of 15 min, reaction temperature of 45 °C, and pH of 3.0.

Furthermore, to survey the high oxidase-like activity of PtNPs/COF-300-AR,

COF-300-AR and unsupported Pt NPs were selected as control catalysts. All the

conditions, including the amount of different catalysts, were the same. From Fig. 3A,

COF-300-AR had a negligible catalytic capacity (black curve). However, after in-situ

forming Pt NPs (blue curve), the catalytic capacity of COF-300-AR was markedly

improved. That is to say, the immobilized Pt NPs are responsible for the excellent

catalytic ability of the nanohybrids. Furthermore, the catalytic ability of 50 μg/mL

PtNPs/COF-300-AR, only having the Pt content of 1.26 μg/mL, was comparable to that

of 50 μg/mL unsupported Pt NPs (pink curve) and far higher than that of 1.26 μg/mL

unsupported Pt NPs (red curve). This was probably owed to the high dispersity and

small size of COF-supported Pt NPs, which was easier to capture and immobilize TMB on the active site. Obviously, COF-supported Pt NPs were significantly superior to unsupported Pt NPs in terms of saving noble metal and reducing aggregation.

Apparent kinetic parameters of the PtNPs/COF-300-AR oxidase mimic was assessed by Michaelis-Menten equation. The corresponding curve was obtained by changing TMB concentration (Fig. 3B), and the calculated apparent values of V_{max} and K_m from Lineweaver-Burk plot (Fig. 3C) were listed in Table S1. Contrast to other enzyme mimics, PtNPs/COF-300-AR had comparable affinity to TMB and reaction speed.
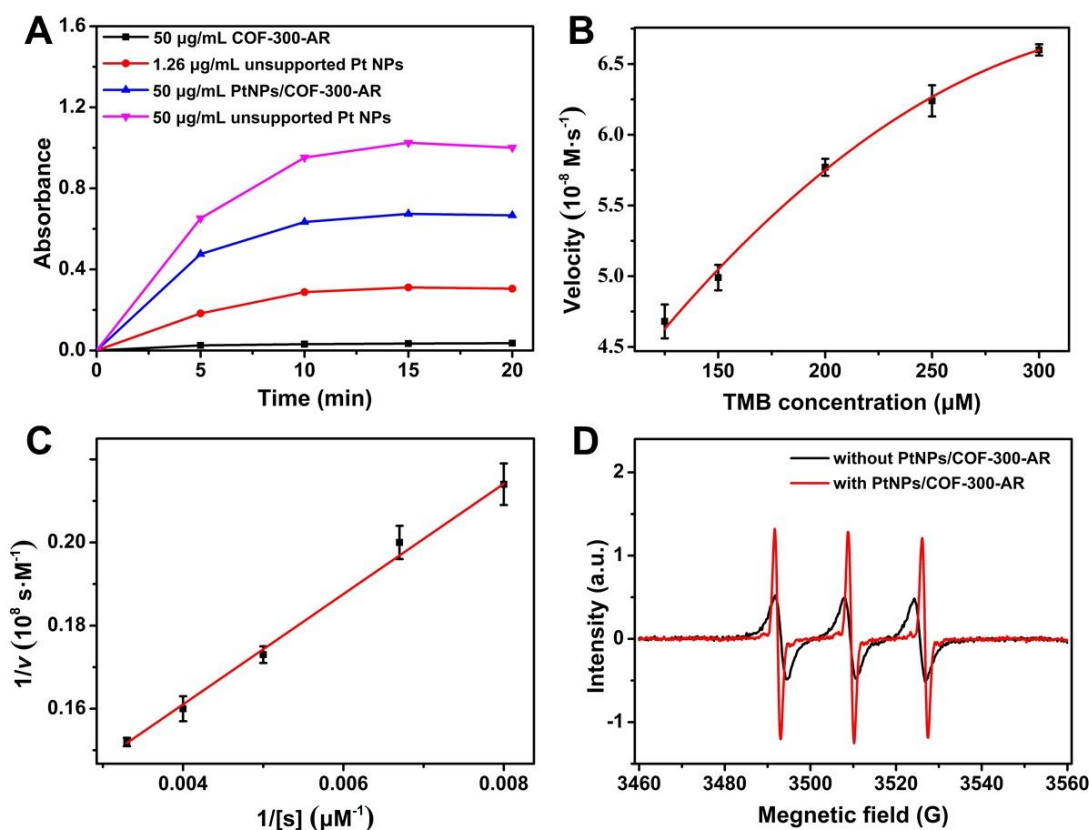

Figure 3. (A) Time course of enzymatic reaction in different catalyst system. (B) Michaelis-Menten curve and (C) Lineweaver-Burk plot of PtNPs/COF-300-AR oxidase

mimic with TMB as substrate. (D) ESR spectra of TEMP solution (0.2 M HAc-NaAc,

pH = 3.0).

3.3. The Catalytic Mechanism of PtNPs/COF-300-AR Oxidase Mimic.

One very critical initiation factor of redox reaction is the existence of oxygen (O_2).

From Table S2, after nitrogen gas blowing the air-saturated solution for 5 min before

reaction, the absorbance at 652 nm decreased by half. Moreover, the absorption signal

was almost completely inhibited after adding a reductant such as ascorbic acid (AA) or

thiourea. These observations clearly indicated that the generation of reactive oxygen

species (ROS) during the catalytic process of the nanohybrids.

To clarify the possible mechanism of PtNPs/COF-300-AR as enzymatic catalyst,

various free radical scavengers were used to probe the presence of ROS. From the

results listed in Table S2, more than 65% absorption intensity was inhibited with the

addition of NaN_3 (100 μM) or histidine (50 μM) which are commonly used $^1O_2$

scavengers. However, suppression was less than 10% with the addition of $O_2{}^{\bullet-}$

scavenger (SOD) and •OH scavenger (ethanol, isopropanol or DMSO). Furthermore,

the ESR spectra were also applied to verify ROS generation with TEMP and DMPO as

$^1O_2$-sensitive (Fig. 3D) and •OH/$O_2{}^{\bullet-}$-sensitive (Fig. S11) trapping agents, respectively,

indicating that $^1O_2$ but not •OH/$O_2{}^{\bullet-}$ was the main ROS. The above results suggest that

$^1O_2$ played a crucial role in the oxidation of TMB, that was consistent with the

significant discovery that $^1O_2$ was generated in the existence of noble metal (Ag, Pd,

Pt, etc.) nanoparticles.[38,51]

Based on the above results, the formed $^1O_2$ could be responsible for the excellent

11

catalytic ability of the PtNPs/COF-300-AR oxidase mimic by oxidizing TMB into its

product (oxTMB), and the possible mechanism is graphically presented in Scheme 1.

3.4. Colorimetric Detection of GSH

The PtNPs/COF-300-AR oxidase mimic was exploited as sensor for the detection

of GSH level. It can be seen in Figs. 4A-B, as GSH concentration increased, the

absorbance at 652 nm gradually decreased, keeping a good linear relationship in the

concentration range (0.4-4.0 μM). GSH with concentration as low as 0.4 μM can be

quantified using our proposed method, which is even comparable with some fluorescent

methods for GSH detection (Table S3). In particular, some possible interferences in cell

lysate, such as amino acids (Gly, Glu, Thr, Arg, L-Leu, Met) and inorganic ions (K^+,

Ca^{2+}, Na^+, NH_4^+, Mg^{2+}, SO_4^{2-}, PO_4^{3-}, HCO_3^-, CO_3^{2-}, $H_2PO_4^-$) showed no

significant effect in GSH detection, except L-cysteine (L-Cys), homocysteine (Hcy),

AA and SO_3^{2-} (Fig. 4C-D). Similar to the most oxidase mimics, the selectivity of

PtNPs/COF-300-AR to GSH is limited, and those substances reacted with ROS radicals

have certain influence on the GSH detection. However, in the cell, GSH is far more

abundant compared to other sulfhydryl compounds,[30,52,53] so our proposed method is

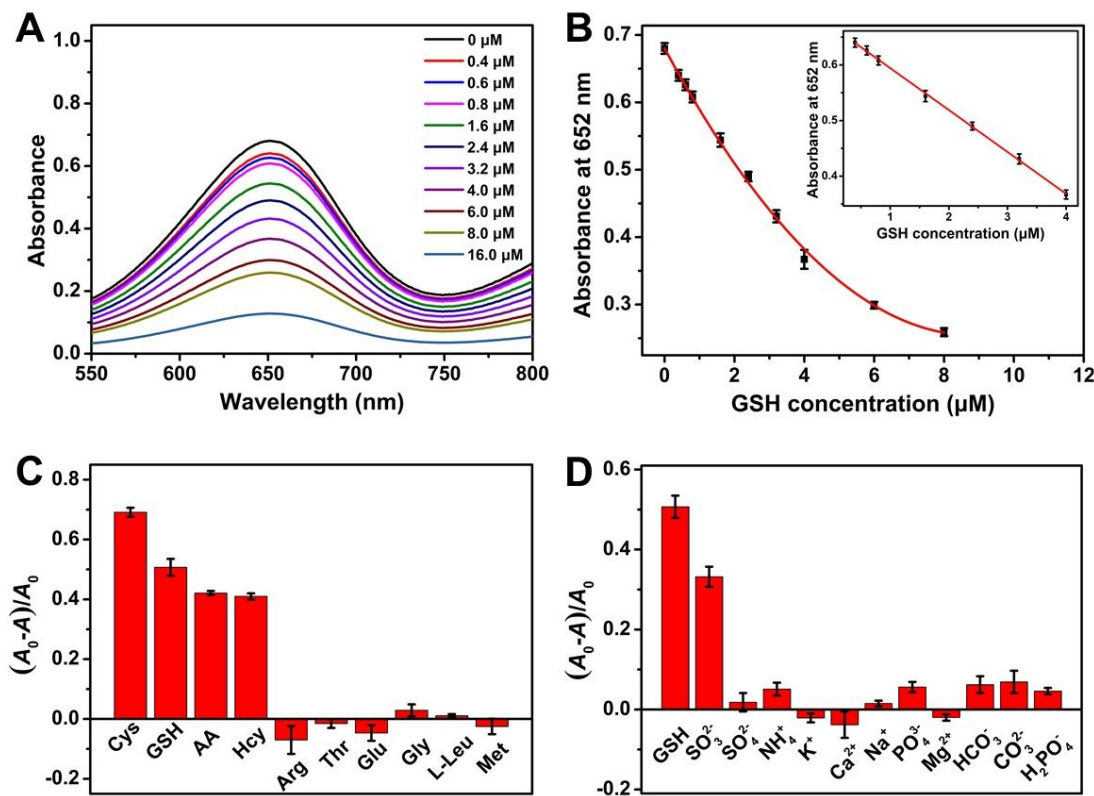perfectly suited to detect cellular GSH.

Figure 4. (A) The change of UV-vis absorption spectra with GSH concentrations (0-16 μM) in the TMB-PtNPs/COF-300-AR system. (B) The relationship between absorbance and GSH concentration (inset is the corresponding linear calibration curve). (C) and (D) show the relative absorption intensity of the proposed method to different analytes (A and A_0 represent the absorbance at 652 nm with and without the analyte, respectively). The concentrations of the analytes are 1 mM except those of L-Cys, Hcy, GSH, AA and SO_3^{2-} (5 μM).

Next, HL60 cell was used as model cell to evaluate the application potential of the nanohybrids in the measurement of cellular GSH level.[54,55] Although the cell lysis buffer had certain effect on the response intensity, there was still a linear relationship between the absorbance and GSH concentrations (1-8 μM), as shown in Fig. S12. In Figs. 5A-B, as the HL60 cell density enlarged from 2×10^4 to 4×10^5, the absorption

13

intensity at 652 nm became weaker owing to the inhibitory feature of cellular GSH toward oxidase-like catalysis. To confirm our proposed assay method, a GSH assay kit was used to assess the GSH level in HL60 cells (Fig. S13). As shown in Fig. 5C, the cellular GSH level measured by the TMB-PtNPs/COF-300-AR system is basically close to that by GSH assay kit, demonstrating our proposed method is very accurate. Therefore, the PtNPs/COF-300-AR nanohybrids was shown to be trustable oxidase mimic for the detection for cellular GSH.

3.5. Reusability and Stability of PtNPs/COF-300-AR.

Finally, the reusability and stability of PtNPs/COF-300-AR oxidase mimic was examined. From Fig. S14, the catalytic activity was still larger than 90% even after 15 days of storage. Moreover, all catalytic activities in a cyclic experiment reached 95% or higher (Fig. 5D), depicting the high reusability and stability of PtNPs/COF-300-AR under high acid buffer solution. The TEM image showed that the reusable PtNPs/COF-300-AR maintained the good morphology after eight cycles, featured by still highly dispersed Pt NPs (Fig. S15). The outstanding reusability and stability of Pt NPs under harsh reaction conditions can be owed to COF-300-AR template, that efficiently stabilized these NPs.
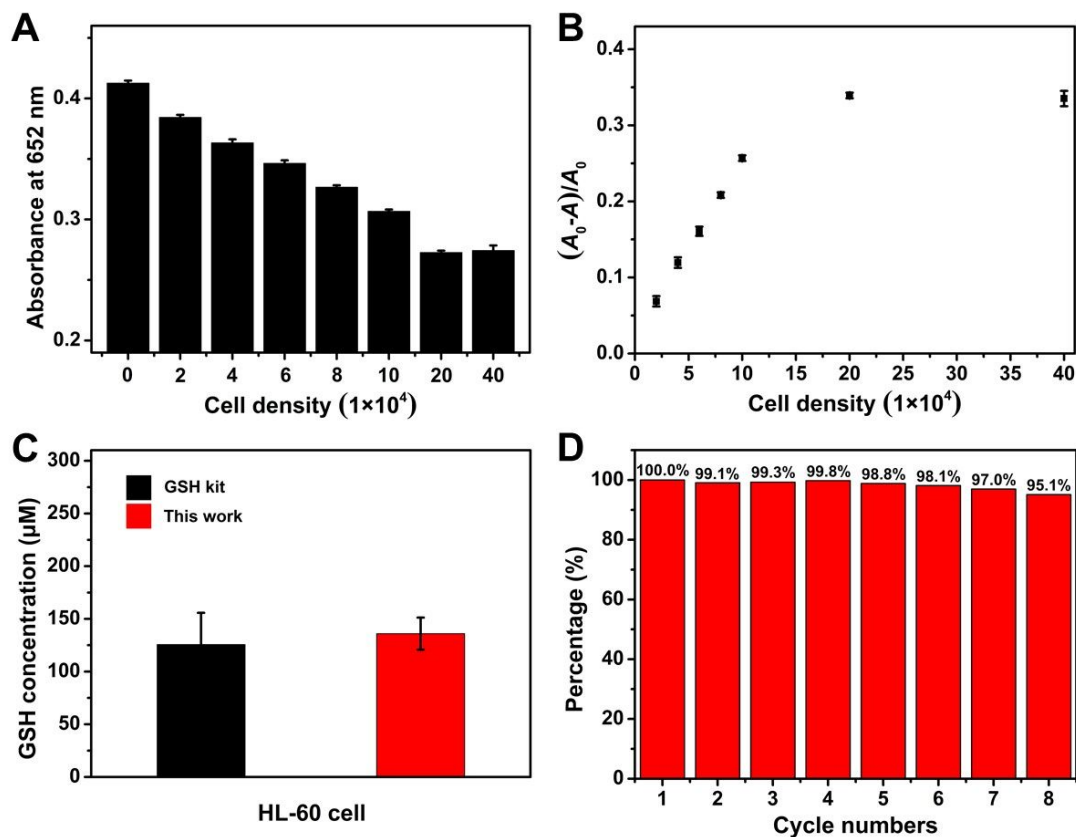
Figure 5. (A) Change of absorbance with HL60 cell density. (B) Correlation of relative absorption intensity and cell density (A and A_0 represent the absorbance at 652 nm with and without HL60 cells, respectively). (C) GSH levels in HL60 cell lysate. (D) Reusability of the nanohybrids in GSH detection.

4. CONCLUSIONS

In brief, we demonstrated excellent oxidase-like catalytic capacity of COF-supported Pt NPs. Benefiting from the introduction of COF-300-AR support, the good dispersity and uniform size of ultrafine Pt NPs were obtained. The as-prepared PtNPs/COF-300-AR nanohybrids showed high affinity to the substrate TMB, illustrating its superior oxidase-like activity. Furthermore, based on construction of the TMB-PtNPs/COF-300-AR platform, a sensitive colorimetric method was established

15

for GSH measurement in cell lysate. This study not only brought porous materials 3D COFs as promising support for construction of artificial enzymes, but also pioneered the application of COF-supported nanozymes and opened promising avenues for more powerful nanozymes.

■ ASSOCIATED CONTENT

Supporting information

Reagents and materials, apparatus, synthesis of COF-300, synthesis of COF-300-AR, oxidase-like activity, catalytic mechanism investigation, cellular GSH measurement, stability, reusability, synthesis of unsupported Pt NPs, measurement of Pt content in PtNPs/COF-300-AR, the procedure of kinetic assay, cell culture and lysate preparation, Figures S1-S15, Tables S1-S3.

■ AUTHOR INFORMATION

Corresponding Authors

Hongli Chen - *State Key Laboratory of Applied Organic Chemistry, College of Chemistry and Chemical Engineering, Lanzhou University, Lanzhou 730000, China;*

E-mail: hlchen@lzu.edu.cn

Hongying Du - *Key Laboratory of Environment Correlative Dietology, Ministry of Education, College of Food Science and Technology, Huazhong Agricultural University, Wuhan, Hubei, China;*

E-mail: hydu@mail.hzau.edu.cn

Authors

Peng Jin - *State Key Laboratory of Applied Organic Chemistry, College of Chemistry and*

16

Chemical Engineering, Lanzhou University, Lanzhou 730000, China;

Xiaoying Niu - *College of Chemistry and Environmental Science, Key Laboratory of Analytical*

Science and Technology of Hebei Province, and MOE Key Laboratory of Medicinal Chemistry

and Molecular Diagnostics, Hebei University, Baoding, Hebei, China;

Zixi Gao - *State Key Laboratory of Applied Organic Chemistry, College of Chemistry and*

Chemical Engineering, Lanzhou University, Lanzhou 730000, China;

Xuqi Xue - *State Key Laboratory of Applied Organic Chemistry, College of Chemistry and*

Chemical Engineering, Lanzhou University, Lanzhou 730000, China;

Fang Zhang - *State Key Laboratory of Applied Organic Chemistry, College of Chemistry and*

Chemical Engineering, Lanzhou University, Lanzhou 730000, China;

Wei Cheng - *State Key Laboratory of Applied Organic Chemistry, College of Chemistry and*

Chemical Engineering, Lanzhou University, Lanzhou 730000, China;

Cuiling Ren - *State Key Laboratory of Applied Organic Chemistry, College of Chemistry and*

Chemical Engineering, Lanzhou University, Lanzhou 730000, China;

Anne Manyande - *School of Human and Social Sciences, University of West London, London,*

UK.

Notes

The authors declare no competing financial interest.

■ **REFERENCES**

(1) Gao, L.; Zhuang, J.; Nie, L.; Zhang, J.; Zhang, Y.; Gu, N.; Wang, T.; Feng, J.; Yang, D.; Perrett, S.; Yan, X. Intrinsic Peroxidase-Like Activity of Ferromagnetic Nanoparticles. *Nat. Nanotech.* **2007**, *2*, 577-583.

(2) Wei, H.; Wang, E. Nanomaterials with Enzyme-Like Characteristics (Nanozymes): Next-Generation Artificial Enzymes. *Chem. Soc. Rev.* **2013**, *42*, 6060-6093.

(3) Wu, J.; Wang, X.; Wang, Q.; Lou, Z.; Li, S.; Zhu, Y.; Qin, L.; Wei, H. Nanomaterials with Enzyme-Like Characteristics (Nanozymes): Next-Generation Artificial Enzymes (II). *Chem. Soc. Rev.* **2019**, *48*, 1004-1076.

(4) Ding, N.; Yan, N.; Ren, C.; Chen, X. Colorimetric Determination of Melamine in Dairy Products by Fe_3O_4 Magnetic Nanoparticles-H_2O_2-ABTS Detection System. *Anal. Chem.* **2010**, *82*, 5897-5899.

(5) Su, L.; Feng, J.; Zhou, X.; Ren, C.; Li, H.; Chen, X. Colorimetric Detection of Urine Glucose Based $ZnFe_2O_4$ Magnetic Nanoparticles. *Anal. Chem.* **2012**, *84*, 5753-5758.

(6) Dutta, A. K.; Maji, S. K.; Srivastava, D. N.; Mondal, A.; Biswas, P.; Paul, P.; Adhikary, B. Synthesis of FeS and FeSe Nanoparticles from a Single Source Precursor: A Study of Their Photocatalytic Activity, Peroxidase-Like Behavior, and Electrochemical Sensing of H_2O_2. *ACS Appl. Mater. Interfaces* **2012**, *4*, 1919-1927.

(7) Roy, P.; Lin, Z. H.; Liang, C. T.; Chang, H. T. Synthesis of Enzyme Mimics of Iron Telluridenanorods for the Detection of Glucose. *Chem. Commun.* **2012**, *48*, 4079-4081.

(8) Zhang, W.; Hu, S.; Yin, J. J.; He, W.; Lu, W.; Ma, M.; Gu, N.; Zhang, Y. Prussian Blue Nanoparticles as Multienzyme Mimetics and Reactive Oxygen Species

Scavengers. *J. Am. Chem. Soc.* **2016**, *138*, 5860-5865.

(9) Baldim, V.; Bedioui, F.; Mignet, N.; Margaill, I.; Berret, J. F. The Enzyme-Like Catalytic Activity of Cerium Oxide Nanoparticles and Its Dependency on Ce^{3+} Surface Area Concentration. *Nanoscale* **2018**, *10*, 6971-6980.

(10) Wu, G. W.; He, S. B.; Peng, H. P.; Deng, H. H.; Liu, A. L.; Lin, X. H.; Xia, X. H.; Chen, W. Citrate-Capped Platinum Nanoparticle as a Smart Probe for Ultrasensitive Mercury Sensing. *Anal. Chem.* **2014**, *86*, 10955-10960.

(11) Liu, Y.; Purich, D. L.; Wu, C.; Wu, Y.; Chen, T.; Cui, C.; Zhang, L.; Cansiz, S.; Hou, W.; Wang, Y.; Yang, S.; Tan, W. Ionic Functionalization of Hydrophobic Colloidal Nanoparticles to Form Ionic Nanoparticles with Enzymelike Properties. *J. Am. Chem. Soc.* **2015**, *137*, 14952-14958.

(12) Deng, H.; He, S.; Lin, X.; Yang, L.; Lin, Z.; Chen, R.; Peng, H.; Chen, W. Target-Triggered Inhibiting Oxidase-Mimicking Activity of Platinum Nanoparticles for Ultrasensitive Colorimetric Detection of Silver Ion. *Chin. Chem. Lett.* **2019**, *30*, 1659-1662.

(13) Huang, M.; Wang, H.; He, D.; Jiang, P.; Zhang, Y. Ultrafine and monodispersed iridium nanoparticles supported on nitrogen-functionalized carbon: an efficient oxidase mimic for glutathione colorimetric detection. *Chem. Commun.* **2019**, *55*, 3634-3637.

(14) Feng, S.; Ming. M.; Wang, M.; Wang, X.; He, D.; Jiang, P.; Chen, Y. Uniformly distributed ruthenium nanocrystals as highly efficient peroxidase for hydrogen peroxide colorimetric detection and nitroreductase for 4-nitroaniline reduction. *Chem. Commun.,* **2020**, *56*, 12347-12350.

(15) Baldim, V.; Bedioui, F.; Mignet, N.; Margaill, I.; Berret, J. F. The Enzyme-Like

Catalytic Activity of Cerium Oxide Nanoparticles and Its Dependency on Ce^{3+} Surface

Area Concentration. *Nanoscale* **2018**, *10*, 6971-6980.

(16) Qin, W.; Su, L.; Yang, C.; Ma, Y.; Zhang, H.; Chen, X. Colorimetric Detection of

Sulfite in Foods by a $TMB-O_2-Co_3O_4$ Nanoparticles Detection System. *J. Agric. Food

Chem.* **2014**, *62*, 5827-5834.

(17) Li, W.; Liu, Z.; Liu, C.; Guan, Y.; Ren, J.; Qu, X. Manganese Dioxide Nanozymes

as Responsive Cytoprotective Shells for Individual Living Cell Encapsulation. *Angew.

Chem. Int. Ed.* **2017**, *56*, 13661-13665.

(18) André, R.; Natálio, F.; Humanes, M.; Leppin, J.; Heinze, K.; Wever, R.; Schröder,

H. C.; Müller, W. E. G.; Tremel, W. V_2O_5 Nanowires with an Intrinsic Peroxidase-Like

Activity. *Adv. Funct. Mater.* **2011**, *21*, 501-509.

(19) Ali, S. S.; Hardt, J. I.; Quick, K. L.; Kim-Han, J. S.; Erlanger, B. F.; Huang, T. T.;

Epstein, C. J.; Dugan, L. L. A Biologically Effective Fullerene (C60) Derivative with

Superoxide Dismutase Mimetic Properties. *Free Radical Biol. Med.* **2004**, *37*, 1191-

1202.

(20) Sun, H.; Zhao, A.; Gao, N.; Li, K.; Ren, J.; Qu, X. Deciphering a Nanocarbon-

Based Artificial Peroxidase: Chemical Identification of the Catalytically Active and

Substrate-Binding Sites on Graphene Quantum Dots. *Angew. Chem. Int. Ed.* **2015**, *54*,

7176-7180.

(21) Lin, T.; Zhong, L.; Wang, J.; Guo, L.; Wu, H.; Guo, Q.; Fu, F.; Chen, G. Graphite-

Like Carbon Nitrides as Peroxidase Mimetics and Their Applications to Glucose

Detection. *Biosens. Bioelectron.* **2014**, *59*, 89-93.

(22) Samuel, E. L. G.; Marcano, D. C.; Berka, V.; Bitner, B. R.; Wu, G.; Potter, A.; Fabian, R. H.; Pautler, R. G.; Kent, T. A.; Tsai, A. L.; Tour, J. M. Highly Efficient Conversion of Superoxide to Oxygen Using Hydrophilic Carbon Clusters. *Proc. Natl. Acad. Sci. U. S. A.* **2015**, *112*, 2343-2348.

(23) Wang, K.; Feng, D.; Liu, T. F.; Su, J.; Yuan, S.; Chen, Y. P.; Bosch, M.; Zou, X.; Zhou, H. C. A Series of Highly Stable Mesoporous Metalloporphyrin Fe-MOFs. *J. Am. Chem. Soc.* **2014**, *136*, 13983-13986.

(24) Lin, T.; Qin, Y.; Huang, Y.; Yang, R.; Hou, L.; Ye, F.; Zhao, S. A Label-Free Fluorescence Assay for Hydrogen Peroxide and Glucose Based on the Bifunctional MIL-53(Fe) Nanozyme. *Chem. Commun.* **2018**, *54*, 1762-1765.

(25) Liu, Y.; Zhou, M.; Cao, W.; Wang, X.; Wang, Q.; Li, S.; Wei, H. Light-Responsive Metal-Organic Framework as an Oxidase Mimic for Cellular Glutathione Detection. *Anal. Chem.* **2019**, *91*, 8170-8175.

(26) Xiong, Y.; Qin, Y.; Su, L.; Ye, F. Bioinspired Synthesis of Cu^{2+}-Modified Covalent Triazine Framework: A New Highly Efficient and Promising Peroxidase Mimic. *Chem. Eur. J.* **2017**, *23*, 11037-11045.

(27) He, J.; Xu, F.; Hu, J.; Wang, S.; Hou, X.; Long, Z. Covalent Triazine Framework-1: A Novel Oxidase and Peroxidase Mimic. *Microchem. J.* **2017**, *135*, 91-99.

(28) Zhou, L.; Luo, X.; Gao, J.; Liu, G.; Ma, L.; He, Y.; Huang, Z.; Jiang, Y. Facile Synthesis of Covalent Organic Framework Derived Fe-COFs Composites as a Peroxidase-Mimicking Artificial Enzyme. *Nanoscale Adv.* **2020**, *2*, 1036-1039.

21

(29) Li, W.; Li, Y.; Qian, H. L.; Zhao, X.; Yang, C. X.; Yan, X. P. Fabrication of a Covalent Organic Framework and Its Gold Nanoparticle Hybrids as Stable Mimetic Peroxidase for Sensitive and Selective Colorimetric Detection of Mercury in Water Samples. *Talanta* **2019**, *204*, 224-228.

(30) Jin, P.; Niu, X. Y.; Zhang, F.; Dong, K.; Dai, H. X.; Zhang, H. G.; Wang, W. F.; Chen, H. L.; Chen, X. G. Stable and Reusable Light-Responsive Reduced Covalent Organic Framework (COF-300-AR) as a Oxidase-Mimicking Catalyst for GSH Detection in Cell Lysate. *ACS Appl. Mater. Interfaces* **2020**, *12*, 20414-20422.

(31) Zheng, X.; Zhu, Q.; Song, H.; Zhao, X.; Yi, T.; Chen, H.; Chen, X. In Situ Synthesis of Self-Assembled Three-Dimensional Graphene-Magnetic Palladium Nanohybrids with Dual-Enzyme Activity through One-Pot Strategy and Its Application in Glucose Probe. *ACS Appl. Mater. Interfaces* **2015**, *7*, 3480-3491.

(32) Soh, M.; Kang, D. W.; Jeong, H. G.; Kim, D.; Kim, D. Y.; Yang, W.; Song, C.; Baik, S.; Choi, I. Y.; Ki, S. K.; Kwon, H. J.; Kim, T.; Kim, C. K.; Lee, S. H.; Hyeon, T. Ceria-Zirconia Nanoparticles as an Enhanced Multi-Antioxidant for Sepsis Treatment. *Angew. Chem. Int. Ed.* **2017**, *56*, 11399-11403.

(33) Liu, J.; Hu, X.; Hou, S.; Wen, T.; Liu, W.; Zhu, X.; Wu, X. Screening of Inhibitors for Oxidase Mimics of Au@Pt Nanorods by Catalytic Oxidation of OPD. *Chem. Commun.* **2011**, *47*, 10981-10983.

(34) Song, N.; Ma, F.; Zhu, Y.; Chen, S.; Wang, C.; Lu, X. Fe_3C/Nitrogen-Doped Carbon Nanofibers as Highly Efficient Biocatalyst with Oxidase-Mimicking Activity for Colorimetric Sensing. *ACS Sustainable Chem. Eng.* **2018**, *6*, 16766-16776.

22

(35) Chen, Y. Z.; Wang, Z. U.; Wang, H.; Lu, J.; Yu, S. H.; Jiang, H. L. Singlet Oxygen-Engaged Selective Photo-Oxidation over Pt Nanocrystals/Porphyrinic MOF: The Roles of Photothermal Effect and Pt Electronic State. *J. Am. Chem. Soc.* **2017**, *139*, 2035-2044.

(36) Liu, Y.; Wu, H.; Chong, Y.; Wamer, W. G.; Xia, Q.; Cai, L.; Nie, Z.; Fu, P. P.; Yin, J. J. Platinum Nanoparticles: Efficient and Stable Catechol Oxidase Mimetics. *ACS Appl. Mater. Interfaces* **2015**, *7*, 19709-19717.

(37) Liu, Y.; Wu, H.; Li, M.; Yin, J. J.; Nie, Z. pH Dependent Catalytic Activities of Platinum Nanoparticles with Respect to the Decomposition of Hydrogen Peroxide and Scavenging of Superoxide and Singlet Oxygen. *Nanoscale* **2014**, *4*, 11904-11910.

(38) Vankayala, R.; Sagadevan, A.; Vijayaraghavan, P.; Kuo, C. L.; Hwang, K. C. Metal Nanoparticles Sensitize the Formation of Singlet Oxygen. *Angew. Chem. Int. Ed.* **2011**, *50*, 10640-10644.

(39) Hamasaki, T.; Kashiwagi, T.; Imada, T.; Nakamichi, N.; Aramaki, S.; Toh, K.; Morisawa, S.; Shimakoshi, H.; Hisaeda, Y.; Shirahata, S. Kinetic Analysis of Superoxide Anion Radical-Scavenging and Hydroxyl Radical-Scavenging Activities of Platinum Nanoparticles. *Langmuir* **2008**, *24*, 7354-7364.

(40) Lee, S. S.; Song, W.; Cho, M.; Puppala, H. L.; Nguyen, P.; Zhu, H.; Segatori, L.; Colvin, V. L. Antioxidant Properties of Cerium Oxide Nanocrystals as a Function of Nanocrystal Diameter and Surface Coating. *ACS Nano* **2013**, *7*, 9693-9703.

(41) Waller, P. J.; Gándara, F.; Yaghi, O. M. Chemistry of Covalent Organic Frameworks. *Acc. Chem. Res.* **2015**, *48*, 3053-3063.

23

(42) Kamai, R.; Kamiya, K.; Hashimoto, K.; Nakanishi, S. Oxygen-Tolerant Electrodes with Platinum-Loaded Covalent Triazine Frameworks for the Hydrogen Oxidation Reaction. *Angew. Chem. Int. Ed.* **2016**, *55*, 13184-13188.

(43) Lu, S.; Hu, Y.; Wan, S.; McCaffrey, R.; Jin, Y.; Gu, H.; Zhang, W. Synthesis of Ultrafine and Highly Dispersed Metal Nanoparticles Confined in a Thioether-Containing Covalent Organic Framework and Their Catalytic Applications. *J. Am. Chem. Soc.* **2017**, *139*, 17082-17088.

(44) Stegbauer, L.; Schwinghammer, K.; Lotsch, B. V. A Hydrazone-Based Covalent Organic Framework for Photocatalytic Hydrogen Production. *Chem. Sci.* **2014**, *5*, 2789-2793.

(45) Tao, R.; Ma, X.; Wei, X.; Jin, Y.; Qiu, L.; Zhang, W. Porous organic polymer material supported palladium nanoparticles. *J. Mater. Chem. A* **2020**, *8*, 17360-17391.

(46) Park, E.; Jack, J.; Hu, Y.; Wan, S.; Huang, S.; Jin. Y.; Maness, P.-C.; Yazdi, S.; Ren, Z.; Zhang, W. Covalent organic framework-supported platinum nanoparticles as efficient electrocatalysts for water reduction. *Nanoscale* **2020**, *12*, 2596-2602.

(47) Tao, R.; Shen, X.; Hu, Y.; Kang, K.; Zheng, Y.; Luo, S.; Yang, S.; Li, W.; Lu, S.; Jin, Y.; Qiu, L.; Zhang, W. Phosphine-based covalent organic framework for the controlled synthesis of broad-scope ultrafine nanoparticles. *Small* **2020**, *16*, 1906005.

(48) Ding, S. Y.; Gao, J.; Wang, Q.; Zhang, Y.; Song, W. G.; Su, C. Y.; Wang, W. Construction of Covalent Organic Framework for Catalysis: Pd/COF-LZU1 in Suzuki-Miyaura Coupling Reaction. *J. Am. Chem. Soc.* **2011**, *133*, 19816-19822.

(49) Kalidindi, S. B.; Oh, H.; Hirscher, M.; Esken, D.; Wiktor, C. J.; Turner, S.;

Tendeloo, G. V.; Fischer, R. A. Metal@COFs: Covalent Organic Frameworks as Templates for Pd Nanoparticles and Hydrogen Storage Properties of Pd@COF-102 Hybrid Material. *Chem. Eur. J.* **2012**, *18*, 10848-10856.

(50) Liu, H.; Chu, J.; Yin, Z.; Cai, X.; Zhuang, L.; Deng, H. Efficient and Selective CO_2 Reduction Integrated with Organic Synthesis by Solar Energy. *Chem* **2018**, *4*, 1-14.

(51) Long, R.; Mao, K.; Ye, X.; Yan, W.; Huang, Y.; Wang, J.; Fu, Y.; Wang, X.; Wu, X.; Xie, Y.; Xiong, Y. Surface Facet of Palladium Nanocrystals: A Key Parameter to The Activation of Molecular Oxygen for Organic Catalysis and Cancer Treatment. *J. Am. Chem. Soc.* **2013**, *135*, 3200-3207.

(52) Hu, G.; Jia, H.; Zhao, L.; Cho, D. H.; Fang, J. Small Molecule Fluorescent Probes of Protein Vicinal Dithiols. *Chin. Chem. Lett.* **2019**, *30*, 1704-1716.

(53) Li, M.; Wu, X.; Wang, Y.; Li, Y.; Zhu, W.; James, T. D. A Near-Infrared Colorimetric Fluorescent Chemodosimeter for The Detection of Glutathione in Living Cells. *Chem. Commun.* **2014**, *50*, 1751-1753.

(54) Jacobson, E. C.L.; Grand, R. S.; Perry, J. K.; Vickers, M. H.; Olins, A. L.; Olins, D. E.; O'Sullivan, J. M. Hi-C Detects Novel Structural Variants in HL-60 and HL-60/S4 Cell Lines. *Genomics* **2020**, *112*, 151-162.

(55) Rudin, D.; Roos, N. J.; Duthaler, U.; Krähenbühl, S. Toxicity of Metamizole on Differentiating HL60 Cells and Human Neutrophil Granulocytes. *Toxicology* **2019**, *426*, 152254.

Table of Contents (TOC) graphic